Desalination and Water Treatment
www.deswater.com
doi: 10.5004/dwt.2021.26569

212 (2021) 173–184
February

Adsorption of Erochrom Black T azo dye by nanocomposite of activated carbon from sugar beet and $LaFeO_3$

Ali Aghashiri, Saeedeh Hashemian*, Forough Kalantari Fotooh

Department of chemistry, Yazd Branch, Islamic Azad University, Yazd, Iran, Tel. +0983187575; Fax: +0983538214810; email: Sa_hashemian@iauyazd.ac.ir (S. Hashemian)

Received 8 February 2020; Accepted 13 September 2020

ABSTRACT

Nanocomposite of organic–inorganic materials was prepared. Activated carbon was prepared by carbonization of sugar beet pulp at 800°C (ACSB). The ACSB@$LaFeO_3$ nanocomposite was prepared by ACSB and nanoparticles of $LaFeO_3$. The structure and surface morphology was studied by Fourier-transform infrared spectroscopy, X-ray diffraction, Brunauer–Emmett–Teller (BET), field emission scanning electron microscopy, and energy-dispersive X-ray spectroscopy methods. BET surface area of ACSB, LaFeO3, and ACSB@$LaFeO_3$ were 825, 15, and 780 m^2/g, respectively. Adsorption of Eriochrome Black-T (EBT) azo dye by ACSB and ACSB@$LaFeO_3$ nanocomposite were investigated. The effect of various parameters such as carbonization temperature, dye concentration, contact time, pH, and dosage of adsorbent were investigated in batch mode. The optimum conditions were obtained at 70 mg/L initial dye concentration, 0.4 g adsorbent dose, and pH of 3. The pseudo-second-kinetic model ($k_2 = 4.54 \times 10^{-2}$ g/mg/min for ACSB@$LaFeO_3$) exhibited better fit than pseudo-first-order and intraparticle diffusion models for the kinetic studies. The Langmuir, Freundlich, and Temkin isotherm models were used for modeling adsorption isotherms. The adjustments of models were confirmed by the Chi-square (χ^2) test and the correlation coefficients (R^2). The Langmuir model appears to be better appropriate for describing the adsorption of EBT. The calculated thermodynamic parameters such as $\Delta G°$, $\Delta H°$, and $\Delta S°$ showed that the adsorption of EBT was feasible, spontaneous, and endothermic at temperature range 288–338 K. ACSB@$LaFeO_3$ nanocomposite can be used as an effective, reusable, low cost, and eco-friendly adsorbent for EBT removal from aqueous solution.

Keywords: Activated carbon; Sugar beet; $LaFeO_3$; Nanocomposite; Dye removal

1. Introduction

Dyes are widely used in the different industries of dyestuffs such as paper, plastics, textile, leather, cosmetics, and food, which generate noticeable amount of wastewater. Most of the dyes have been considered as harmful organic compounds for environment, because the residual of dyes are resistant to biodegradation processes [1]. Azo dyes are an interesting class of compounds that are widely used in industries, chemical applications, and textile dyeing processes. Furthermore, removal of the azo dyes from the effluent is difficult because they are not easily degradable or removable by conventional wastewater treatments [2]. Hence, removal of untreated effluents to the surrounding environment often leads problems for aquatic life and humans. To prevent any potential hazards, effective treatment methods are needed before discharged of these industrial wastewaters into the environment [3]. Numerous technologies now are to overcome effluent-contain-dye problem such as coagulation and flocculation [4], biosorption [5], membrane [6], advanced oxidation [7], photodegradation [8], and adsorption [9–12] have been usually applied in the process of removing dyes from aqueous solution.

* Corresponding author.

Among various treatment methods, adsorption is quite a promising technique for the removal of dyes due to its high efficiency, ease of handling, availability of different adsorbents, and its cost-efficiency. Activated carbon is highly effective adsorbent for the removal of dyes. But, high cost of commercially available activated carbon, high operating cost, and problems with regeneration, prevent the use of activated carbon for large-scale applications. To minimize the cost of producing activated carbon, we can use low-cost precursors such as agricultural waste. This has focused many researchers on the examination of low-cost adsorbents such as natural agro-industrial or plant waste materials for the removal of dyes and other contaminants from wastewaters. Indeed agricultural wastes have potential in the manufacturing of adsorbents due to its abundance and renewability [13]. Variety of biomass wastes such as waste almond shell and orange peel [14], rice husk [15], waste potato [16], sunflower piths [17], waste carpets [18], tomato stem [19], palm petiole [20], and coffee grounds [21] have been used to produce adsorbents. Sugar beet pulp also is low-cost agro-waste precursor for production of activated carbon [22,23]. Eriochrom Black T (EBT) azo dye was removed by different methods such as catalytic Fenton oxidation [24] and adsorption [25–27].

Perovskite-type materials with the general formula of ABO_3 have attracted considerable attention in the field of catalysis. $LaFeO_3$-type perovskite is one of the most important materials and has attracted attention because of their wide applications, such as electrodes materials for fuel cells, catalysts, chemical sensors, and optoelectronic devices [28,29]. It is reported that perovskite oxide exhibits high adsorption and photocatalytic activity toward degradation of organic contaminant under visible light irradiation and stable in various environment [30]. Therefore, perovskite oxide with appropriate crystal structure, morphology, and optical properties for improvement of catalytic efficiency is paid much attention by researchers.

The cost-effective material that was examined as sorbent material for uptake of EBT dye is activated carbon from sugar beet. In the current study, sugar beet pulp based activated carbon was prepared by using calcination method. The nanocomposite of $LaFeO_3$ mixed oxide and activated carbon from sugar beet was prepared. The as prepared composite was used for adsorption of EBT dye from aqueous solutions. Adsorption was evaluated as a function of various parameters such as pH, contact time, and dose of sorbent. The kinetic modes such as pseudo-first-order, pseudo-second-order, and intraparticle diffusion were studied for adsorption of EBT on the adsorbent's surface. Langmuir, Temkin, and Freundlich adsorption isotherm models were also investigated. Thermodynamic parameters of the adsorption process have been studied and the important parameters such as the changes in Gibbs free energy, entropy, and enthalpy of adsorption were determined. Desorption of sorbent also was studied.

2. Experimental setup

2.1. Materials

Iron nitrate ($Fe(NO_3)_3{\cdot}9H_2O$), lantanium nitrate ($La(NO_3)_3{\cdot}6H_2O$), and citric acid or 2-hydroxypropane-1,2,3-tricarboxylic acid ($C_6H_8O_7$) were purchased from Merck (Germany) and used without further purification. Analytical grade reagents were used in all experimental. EBT was purchased from Sigma-Aldrich (India).

2.2. Methods

EBT ($C_{20}H_{12}N_3NaO_7S$) is an azo dye with a molecular weight 461.38. (IUPAC name is 1-[1-hydroxy 2-naphthol azo]-6-nitro-2-naphthol-4-sulfonic acid sodium salt) and color index 14645. The standard solutions of 1,000 mg L^{-1} of EBT were prepared and subsequently whenever necessary, diluted. The structure of the EBT azo dye is shown in Fig. 1. Analytical grade reagents were used in all experimental. All of compounds were used as received, without any further purification. Distilled water was used in all of the experiments.

$LaFeO_3$ was prepared through a sol–gel method [28]. In a typical procedure, 0.06 mol (38.42 g) of ($Fe(NO_3)_3{\cdot}9H_2O$), 0.06 mol (25.98 g) $La(NO_3)_3{\cdot}6H_2O$, and 0.2 mol (38.426 g) citric acid ($C_6H_8O_7{\cdot}H_2O$) were dissolved in 400 mL of deionized water. The solution was stirred for 1 h at 70°C and then heated to evaporate the water at the same temperature. The gel precursor was dried in air at 150°C for 5 h, and the resulting material was heated in air for room temperature to 800°C at a rate of 3°C/min and calcined at this temperature from 4 h [30].

The sugar beets were placed in porcelain crucibles and heated in a tube furnace for 2 h at different temperatures (100°C–1,100°C) at a heating rate of 5°C/min.

The ACSB@$LaFeO_3$ nano composite was prepared as the same method. Nano composite with ratio of ACSB: $LaFeO_3$ 10:1 was prepared. 10 g of $ACSB_{800}$ and 1 g of $LaFeO_3$ nano particles were mixed, stirred, and reflexed for 2 h at 70°C and then heated and calcinated. The prepared ACSB@ $LaFeO_3$ nano composite was dried at 80°C for 3 h.

2.3. Characterization

The analyses of surface samples such as average particle size and morphology of samples were observed by field emission scanning electron microscopy (FESEM) using a MRIA3 TESCAN-XMU microscope (USA) (equipped with microanalysis dispersion X-ray (EDS) for its quantification). Fourier transform infrared spectroscopy (FTIR) analysis was undertaken on a tensor-27 Bruker infrared spectrometer (Germany). The spectra were recorded in the

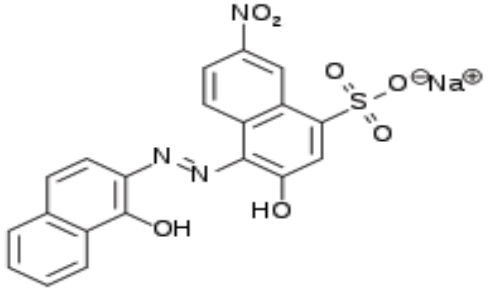

Fig. 1. Molecular structure of EBT.

range, 400–4,000 cm^{-1}, using a pressed KBr pellet technique. pH of solution were adjusted by WTW (Germany) pH meter. Concentration of EBT was determined using the HACH DR 6000™ UV-vis spectrophotometer (USA). The Brunauer–Emmett–Teller (BET) surface area of the samples was determined by N_2 adsorption–desorption measurements using a Quantachrome Nova 2000e instruments. The phase and crystal structure of samples was determined via the X-ray powder diffraction (XRD, Pw3040 Philips, Netherlands) using Cu Kα (λ = 1.542 Å) radiation in the scan range from 5° to 80°. Magnetization measurements of nickel titanate and zeolitic imidazolate framework supported on nickel titanate nanocomposites were performed using vibrating sample magnetometer (VSM-BHV-55, Riken, Japan) at room temperature.

2.4. Adsorption experiments

The adsorption studies were carried out at 25°C ± 1°C in a horizontal shaker using 100.0 mL Erlenmeyer flasks containing 50.0 mL of the test solution with a known EBT concentration by shaking at150 rpm for period contact time. Batch adsorption method was used for experiments. The effect of contact time, solution pH, initial dye concentration, and sorbent dosage were examined. Samples were kept at fixed time intervals (0–75 min). The pH of dye solutions were adjusted with HCl 0.1 M or NaOH 0.1 M. The mixtures were separated by a magnet and then, filtered through 0.45 mm filters. The residual EBT concentration in the supernatant was determined using UV-vis spectrophotometer at λ_{max} 530 nm. The removal efficiency of the EBT molecules was calculated from the difference between the concentrations of EBT before and after sorption using the following Eq. (1):

$$R = \left(\frac{C_i - C_e}{C_i}\right) \times 100 \quad (1)$$

where R is the removal efficiency (%) of the EBT, and C_i and C_e are the initial and equilibrium (residual) concentrations of EBT (mg/L), respectively. The adsorption capacity of EBT (q) was determined according to Eq. (2):

$$q_e = \frac{(C_i - C_e)V}{M} \quad (2)$$

where q_e is the adsorption capacity of EBT (mg/g), C_i and C_e are the initial and final EBT concentrations in the solution (mg/L), V is solution volume (L), respectively, and M is the mass of sorbent (g). Each experiment was repeated three times, and the results are given as averages.

3. Results and discussion

3.1. Characterization studies

The morphology of the sorbents was studied by FESEM. Fig. 2 shows the FESEM images of sugar beet, carbonized sugar beet at 800°C (ACSB), ACSB@$LaFeO_3$ composite, and ACSB@$LaFeO_3$ after EBT dye adsorption. Fig. 1 shows the structure of raw sugar beet and it is clear that sugar beet particles were assemblage of fine particles, which did not have regular and fixed shape and size. The figure shows the structure of ACSB and exhibit fiber-like structures. The FESEM also clearly shows that the ACSB@$LaFeO_3$ is mostly irregular in shape and porous which exhibits pores and gaps. The surface of ACSB@$LaFeO_3$ adsorbent before EBT adsorption is different from the surface of EBT-loaded adsorbent which confirms that the surface of ACSB@$LaFeO_3$ is covered with dye molecules. The images also show the surface morphology of sugar beet was different from that of ACSB, ACSB@$LaFeO_3$, and ACSB@$LaFeO_3$ after EBT adsorption. It looks like the surface of ACSB@$LaFeO_3$ nanoparticles swelled by dye molecules.

The porous active sites distinguished on the surface layer of ACSB@$LaFeO_3$ may increase the specific surface area and lead to faster action of adsorption.

Elemental analysis of ACSB and ACSB@$LaFeO_3$ was carried out, in order to determine the percentage weight of chemical compositions available on the surface, through energy dispersive X-ray spectrometer (EDX) analysis. (ACSB; C: 82.49%, O: 10.9%, K: 3.2%, Ca: 2.6% and ACSB@$LaFeO_3$; C: 65%, O: 21.8%, Fe: 3.1%, La: 8%, K: 0.6%, Ca: 0.55%). According to the results, the highest amounts corresponded to the carbon and the oxygen which evidence the organic nature of the ACSB adsorbent.

The FTIR spectra of $LaFeO_3$ and ACSB@$LaFeO_3$ are shown in Fig. 3. The absorption band around 3,400 cm^{-1}

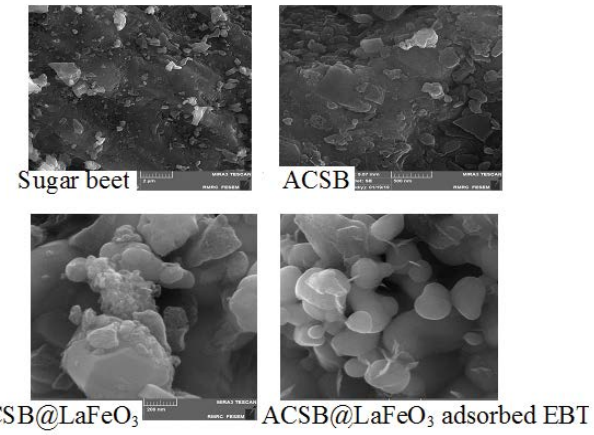

Fig. 2. FESEM of (a) sugar beet, (b) carbonized sugar beet at 800°C (ACSB), (c) ACSB@$LaFeO_3$, and (d) ACSB@$LaFeO_3$ adsorbed EBT.

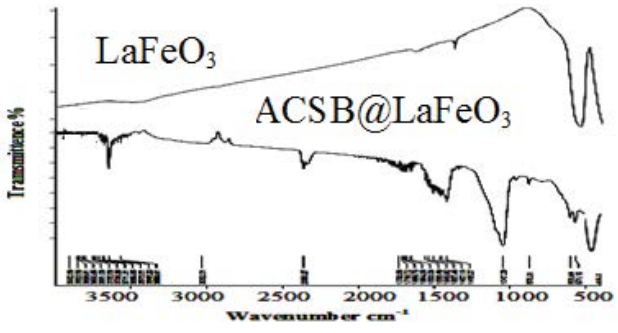

Fig. 3. FTIR of $LaFeO_3$ and ACSB@$LaFeO_3$.

appeared in the IR spectra corresponded to OH stretching of water. The small absorption band at 1,408 cm^{-1} was corresponded to nitrate ion (Fig. 3a). The absorption band at ~560 cm^{-1} is ascribed to La–O/Fe–O stretch vibrations in the perovskite structure [30]. The FTIR spectrum of ACSB@$LaFeO_3$ is shown in Fig. 3b. The peak at 3,550 cm^{-1} is characteristic of the stretching vibration of hydrogen bonded to the –OH groups. The signal at 2,450 cm^{-1} was assigned to the C:C (alkynes). The bands between 1,640 and 1,400 cm^{-1} are assigned to the carbonyl group. The band around 1,047 cm^{-1} was assigned to C=O functional groups of anhydrides. The FTIR analysis revealed the presence of many surface functional groups such as hydroxyl groups and carbonyl group [1]. The band of around 550 cm^{-1} about La–O/Fe–O also is appeared in the composite spectrum.

Fig. 4 shows the XRD patterns of ACSB@$LaFeO_3$ nanocomposite. The X-ray diffraction pattern of nanocomposite shows the characteristic reflection of Perovskite type oxides of $LaFeO_3$ with an orthorhombic structure (a = 5.5669, b = 7.8547, c = 5.5530, $\alpha = \beta = \gamma = 90$, primitive and its space group was Pnma). The diffraction data is in agreement with the JCPD card for $LaFeO_3$ (JCPDS No. 69 37-1493) [31].

Patterns appeared at 2θ = 32° (011), 40° (012), and 45° (202) also confirmed the presence of ACSB. The results also shows peresence of ACSB did not change the structure and crystal phase of $LaFeO_3$ and both of phases of ACSB and $LaFeO_3$ were observed.

The magnetic property of ACSB@$LaFeO_3$ nano composite was investigated by vibrating sample magnetometer (VSM). At room temperature, the hysteresis loop of ACSB@$LaFeO_3$ nano composite is shown at Fig. 5 in the range of ±15 kOe. The VSM of ACSB@$LaFeO_3$ nano composite shows antiferromagnetic and insulator behavior in room temperature. The ACSB@$LaFeO_3$ had negligible remanence and coercivity. At the room temperature M(H) curve is linear. The ACSB@$LaFeO_3$ had saturation magnetization (M_s) of 0.67 emu/g and remnant magnetization (M_r) of 0.18 emu/g, coercive field. The $LaFeO_3$ nanoparticles showed weak antiferromagnetic behavior [31].

The specific surface area of ACSB, $LaFeO_3$, and ACSB@$LaFeO_3$ was determined by BET. BET surface area of ACSB, $LaFeO_3$, and ACSB@$LaFeO_3$ were 825, 15, and 780 m^2/g, respectively.

3.2. Adsorption studies of EBT azo dye

In this research adsorption of EBT dye on the ACSB@$LaFeO_3$ was studied. The factors affecting the adsorption capacity (factors related to adsorbent and factors related to adsorbate) are discussed in details.

3.2.1. Effect of carbonization temperature and contact time

The activated carbon from sugar beet (ACSB) was prepared at various temperatures (100°C–1,100°C). The removal of EBT was tested by different ACSBs. Results showed the $ACSB_{800}$ had the highest percentage removal of EBT from aqueous solutions. Thus, the 800°C was selected as the best temperature for carbonization of sugar beets.

The impact of contact time on the adsorption process of EBT onto ACSB@$LaFeO_3$ composite was studied with 50 mL of EBT with initial concentration of 70 mg/L. It can be observed the adsorption increases with the increasing of stirring time. As shown in Fig. 6a, the adsorption capacity for EBT by ACSB and ACSB@$LaFeO_3$ composite increased quickly until 50 and 25 min, respectively, and then increased gradually. It was found that more than 90% adsorption of dye occurred in the first 50 and 25 min for ACSB and ACSB@$LaFeO_3$, respectively; thereafter the rate of adsorption was found to be slow. This shows that equilibrium can be assumed to be achieved after 50 and 25 min. It is mainly due to saturation of the active sites which does not permit more adsorption to take place. The reason for this observation is the presence of a concentration gradient in the first period of adsorption which increases the amount of dye adsorbed. Then, dye molecules are associated in the adsorption site and the available sites decrease. Therefore, the amount of adsorbed dye almost is constant

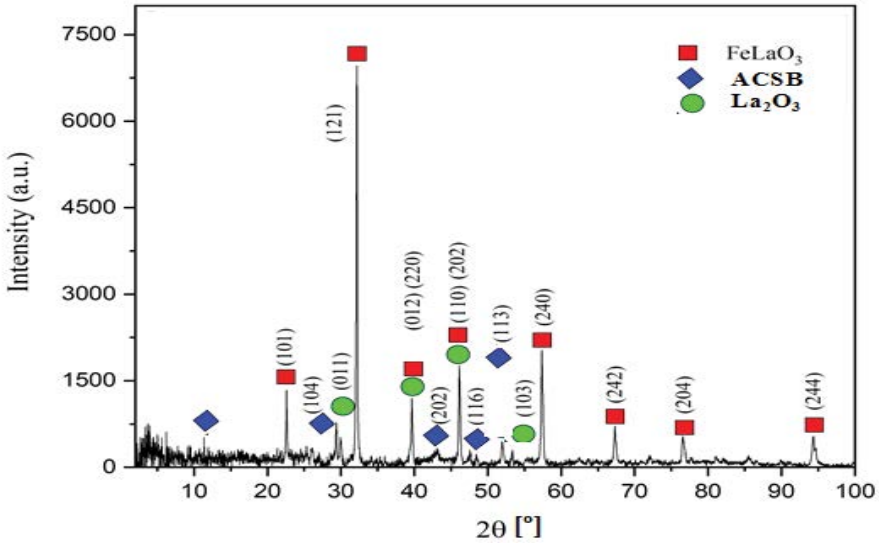

Fig. 4. XRD patterns of ACSB@$LaFeO_3$.

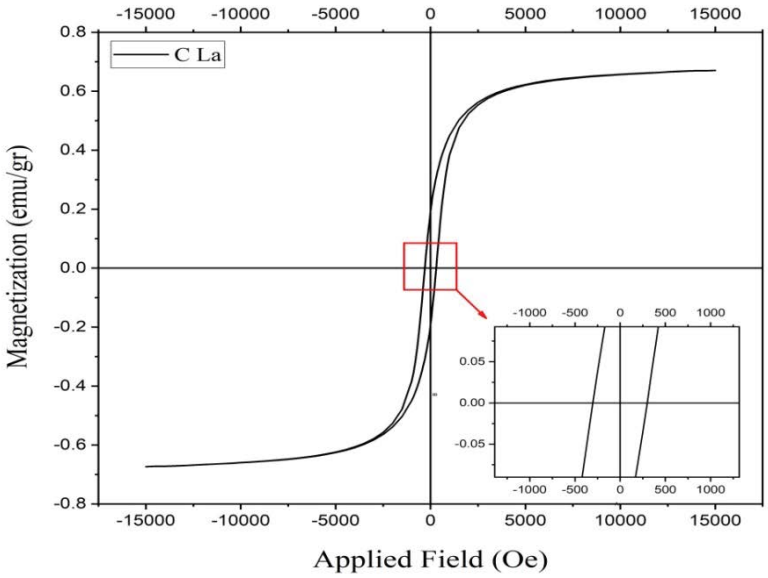

Fig. 5. VSM of ACSB@$LaFeO_3$ nanocomposite.

[32]. The results also showed the ACSB@$LaFeO_3$ nano composite has higher adsorption capacity for EBT from aqueous solutions. It is may be due to catalytic effect of $LaFeO_3$ on the ACSB for dye removal.

FTIR of ACSB@$LaFeO_3$ adsorbed EBT dye is shown in Fig. 6b. The broad band at 3,421 cm^{-1} for distinguished for the stretching vibration of –OH group. The FTIR also shows the bands of M–O (La–O/Fe–O) are appeared around 550 cm^{-1} and the structure of ACSB@$LaFeO_3$ did not change after adsorption of EBT dye. The peaks at 2,920 indicated C–H stretching. The bands about 1,650 are due to the existence of carbonyl group that is broadened. This is may be due to vigorous interaction of dye with these groups. This might be due to the adsorption of EBT and attachment of dye molecules to the binding sites on the surfaces of sorbent. Generally, electrostatic interactions, covalent, and hydrogen bond are the main mechanisms involved in the adsorption of organic compounds on the surface of carbon based adsorbents [27]. Probably, the formation of complex structure after adsorption of EBT molecules on the surface of ACSB@$LaFeO_3$ has affected their peak intensities.

3.2.2. *Effect of pH*

The pH of the aqueous solution is an important controlling parameter in the adsorption process. The effect of initial pH on the adsorption of EBT onto activated carbon form sugar beet (ACSB) and ACSB@$LaFeO_3$ nanocomposite was examined at different pHs (3–10). Results are shown in Fig. 7. When the pH increased from 3 to 10, the adsorption capacity decreased. The maximum adsorption of EBT was observed at pH 3.0. Hence, all the following investigations were performed at pH 3.0.

Sugar beet contains of 65%–80% polysaccharides, consisting roughly of 40% cellulose, 30% hemicelluloses, and 30% pectin [4].

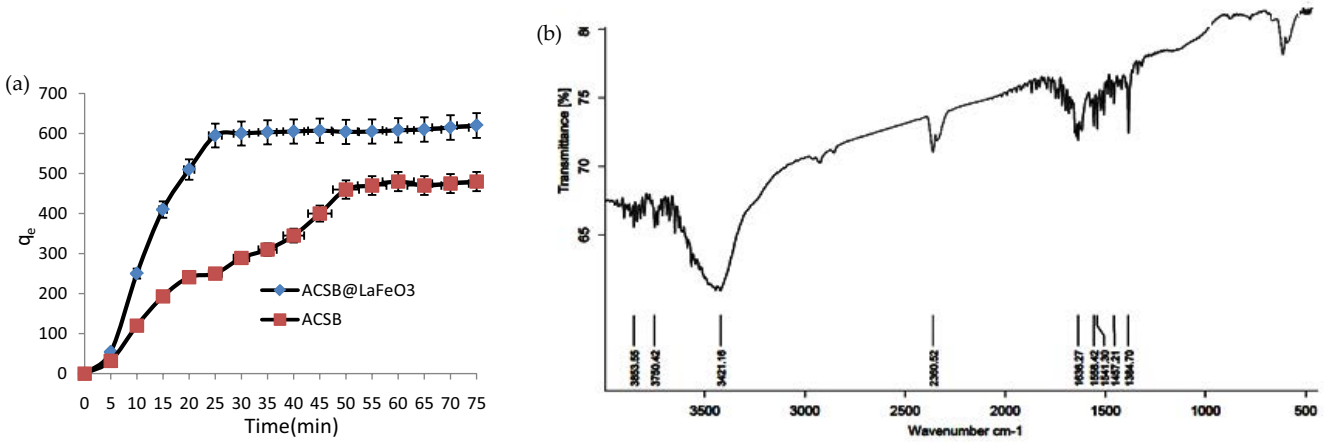

Fig. 6. (a) Effect of contact time for adsorption of EBT onto ACSB and ACSB@$LaFeO_3$ (50 mL of EBT of 70 mg/L, 0.4 g sorbent at 25°C). (b) FTIR of ACSB@$LaFeO_3$ after adsorption p of EBT.

The effect of pH on the adsorption of EBT by activated carbon can be manifested by two mechanisms: an electrostatic interaction between the functional groups of carbon and EBT or a chemical reaction between the adsorbent and the adsorbate. Indeed, the activated carbon surface contains carboxylic and phenolic functions. The dissociation of dye takes place depending on pH values. At pH 3.0 a significantly high electrostatic attraction exists between the positively charged surface of the adsorbent and EBT anionic dye.

Indeed, the phenolic groups of sorbents are protonated and attract the anionic dye due to electrostatic forces of interaction. A significantly high electrostatic attraction exists between the positively charged surface of the adsorbent and anionic dye. This suggests that chemisorption is the model of adsorption at low pH. As the pH of the system increases, the number of negatively charged sites increases, and the number of positively charged sites decrease. Therefore, there are no additional exchangeable anions on the outer surface of the adsorbent at higher pH and thus the observed decreased of adsorption. A negatively charged surface site on the adsorbent does not favor the adsorption of the dye anions due to the electrostatic repulsion. Also, lower adsorption at higher pH may be due to the additional of OH^- ions and causing ionic repulsion between the negatively charged surface and the anionic dye molecules. Therefore, there are no more exchangeable anions on the outer surface of the adsorbent at higher pH and thus the observed decreased adsorption. A similar type of behavior is also reported for adsorption of azo dyes with different adsorbents [33].

The effect of ionic strength on adsorption of EBT by ACSB@$LaFeO_3$ at pH 3.0, 70 mg/L of EBT, and 25°C was investigated. Ionic strength was examined by sodium chloride 0.1–1 mol/L. The results show a weak influence of the ionic strength, as the capacity of adsorption declined slightly due to the competition between EBT and chloride anions of sodium chloride for the active sites from the solid surface. With increasing the concentration of sodium chloride from 0.1 to 1 mol/L, the adsorption capacity of EBT decreases slightly.

3.2.3. Determination of point of zero charge

The point of zero charge (PZC) of ACSB@$LaFeO_3$ sorbent was determined by addition of 20 mL of 1–5 M NaCl to a series of 100 mL of Erlenmeyer flasks and the pH_i values of each solution by adding each of HCl or NaOH were adjusted at values from 2 to 12 [34]. The pH_i of the solutions was then accurately noted and 0.2 g of sorbent was added to each flask. The suspensions were then shaken for 24 h, and the final pH values of the supernatant were measured. The difference between the initial and final pH value, ΔpH ($pH_i - pH_f$), was plotted vs. pH_i. The intersection point of the resulting null ΔpH corresponds to the PZC [33]. The value of PZC of ACSB@$LaFeO_3$ sorbent was determined to be 3.8 ± 0.1. At pH < PZC the H^+ ion concentration increase in the system and the surface of the ACSB@$LaFeO_3$ sorbent gains positive charges by absorbing H^+ ions, which allow a strong electrostatic attraction between the positively charged ACSB@$LaFeO_3$ sorbent surface and the negatively charged EBT molecules leading to maximum adsorption of dye at low pH. At pH > PZC the ACSB@$LaFeO_3$ adsorbent surface is negatively charge which disfavored the adsorption of the negatively charged EBT molecules due to the electrostatic repulsion. So, EBT adsorption onto ACSB@$LaFeO_3$ nanocomposite is favored at pH lower than 3.8.

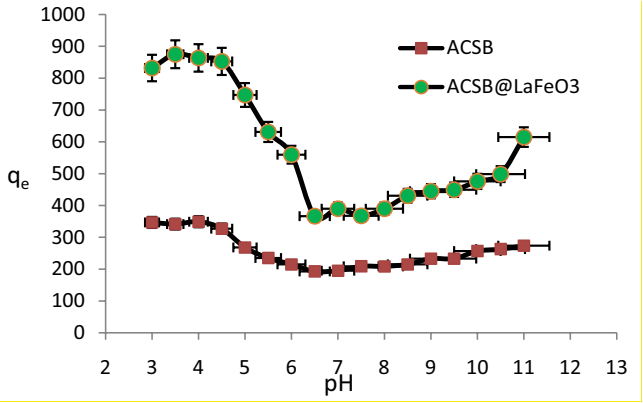

Fig. 7. Effect of pH for adsorption capacity of EBT by ACSB@$LaFeO_3$ (50 mL of EBT of 70 mg/L, 0.4 g sorbent at 25°C).

3.2.4. Effect of the mass of adsorbent

Adsorption is strongly influenced by amount of the adsorbent. The effect of the mass of sorbent on the adsorption of EBT by ACSB@$LaFeO_3$ was studied by varying the mass from 0.1 to 1 g for samples at a constant stirring rate of 25 min with 50 mL of optimum dye concentration of 70 mg/L. Increasing the mass of the sorbent from 0.1 to 0.4 g leads to an increase in adsorption capacity of ECT dye. This is due to the fact that with increasing amount of sorbents more surface area is available for adsorption due to increasing the number of active sites on the adsorbent. For amounts more than of 0.4 g of sorbent, the EBT removal remains almost unchanged. Upon reaching an adsorbent amount of 0.4 g a state of equilibrium was observed featuring a maximum in the adsorption of EBT. This seems to be related to an increase in the number of adsorption sites. Thus, the optimum mass for the further study of adsorption of EBT by ACSB@$LaFeO_3$ will be 0.4 g.

3.3. Adsorption kinetics

The pseudo-first-order (Langergren and Svenska [35]) and pseudo-second-order equations (Ho and McKay [36]) and intraparticle diffusion were considered for adsorption kinetics models of EBT by ACSB and ACSB@$LaFeO_3$ in present study [37,38].

To evaluate the effect of contact time on the adsorption, the same steps described previously were followed. 0.4 g of adsorbent were agitated with 50 mL of the EBT solution (70 mg/L) at 25°C and solution pH 3 for the chosen contact time ranging from 0 to 80 min.

The pseudo-first-order model and pseudo-second-order model kinetics equations were defined as Eqs. (3) and (4):

$$\ln\left(q_e - q_t\right) = \ln q_e - k_1 t \tag{3}$$

$$\frac{t}{q_t} = \frac{t}{q_e} + \frac{1}{\left(k_2 q_e^2\right)} \tag{4}$$

where q_e and q_t represent the amount of EBT adsorbed (mg/g) at equilibrium and at any time, k_1 is the rate constant pseudo-first-order mode of adsorption (1/min), k_2 in the rate constant of the pseudo-second-order equation (g/mg/min).

When $\ln(q_e - q_t)$ was plotted against time, a straight line should be obtained with a slope of k_1, if the first-order kinetics is valid. A plot of t/q_t vs. time (t) would yield a line with a slope of $1/q_e$ and an intercept of $1/(k_2 q_e^2)$, if the second-order model is a suitable expression (Fig. 6). The adsorption data were fitted using the plots of $\ln(q_e - q_t)$ against t for pseudo-first-order model and t/q_t vs. t for pseudo-second-order model (Fig. 7; Table 1).

The intraparticle diffusion equation is given as [39]:

$$q_t = k_3 t^{1/2} + C \tag{5}$$

where q_t (mg/g) is the amount of solute on the surface of the sorbent at time t and k_3 (mg/g min$^{1/2}$) is the intra-particle diffusion rate constant.

The intraparticle diffusion rate constant k_3 was calculated from the slop of the line obtained by plotting q_t and $t^{1/2}$. From the intraparticle diffusion plot shown in Fig. 8, it was obvious that the adsorption processes followed two steps. Table 1 shows the rate constant of intraparticle diffusion and R^2. The kinetic model with a higher correlation coefficient (R^2) was selected as the appropriate one. From the fitting process, pseudo-second-order model shows a good agreement with experimental data.

3.4. Adsorption isotherm

The equilibrium adsorption isotherms are one of the promising data to understand the mechanism of the adsorption. The adsorption equilibrium isotherms successfully represent the dynamic adsorptive separation of solute from solution. The most commonly applied isotherms, in solid/liquid system, are Langmuir, Freundlich, and Temkin isotherms [40,41]. The Freundlich isotherm model assumes a multilayer adsorption on heterogeneous surface with interaction between adsorbed molecules. The Freundlich model was chosen to estimate the adsorption intensity of the sorbate on the sorbent surface. The model is expressed as follows:

$$q_e = K_F C_e^{1/n} \tag{6}$$

$$\log q_e = \log K_F + \frac{1}{n}\log C_e \tag{7}$$

where q_e is the equilibrium adsorption capacity of the sorbent (mg/g), C_e is the equilibrium concentration of EBT (mg/L), and K_F (mg/L) and $1/n$ are Freundlich constants related to the sorption capacity and intensity, respectively. The intercept K_F obtained from the plot of $\log q_e$ vs. $\log C_e$ is roughly a measure of the sorption capacity and the slope ($1/n$) of the sorption intensity (Fig. 9).

The Langmuir equation was chosen for the estimation of maximum adsorption capacity corresponding to complete monolayer coverage on the adsorbent surface.

The Langmuir isotherm assumes that the maximum adsorption exists when saturated monolayer coverage of the adsorbate is present on the adsorbent surface. The Langmuir model also assumes that adsorption occurs at specific homogeneous sites within the adsorbent and there is no important interaction among the adsorbed species. The Langmuir isotherm model is expressed by the following equations:

$$q_e = \frac{q_{\max} K_L C_e}{\left(1 + K_L C_e\right)} \tag{8}$$

$$\frac{C_e}{q_e} = \frac{1}{\left(q_{\max} K_L\right)} + \frac{C_e}{q_{\max}} \tag{9}$$

where q_e (mg g^{-1}) is the amount adsorbed at equilibrium, $q_{\max}$ (mg g^{-1}) is the adsorption capacity, C_e (mg L^{-1}) is the concentration of the solution at equilibrium, K_L (L mg^{-1}) is the Langmuir constant (Fig. 10).

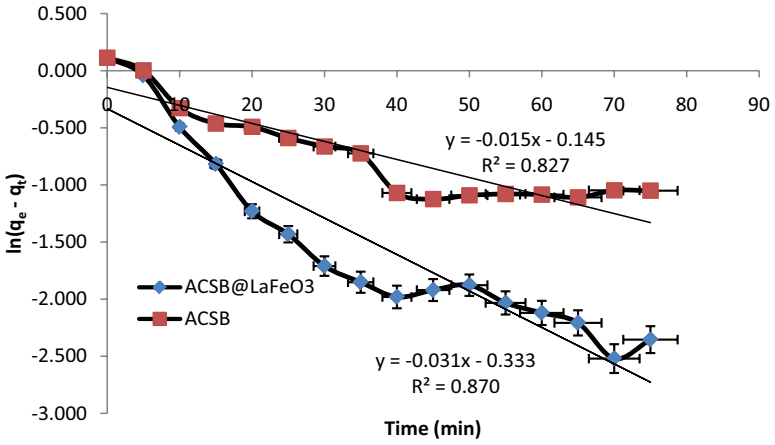

Fig. 8. Pseudo-first-order kinetic model for adsorption of EBT by ACSB and ACSB@LaFeO$_3$ (50 mL of EBT of 70 mg/L, pH 3, and 0.4 g sorbent at 25°C).

Table 1
Kinetics constants for the adsorption of EBT on ACSB and ACSB@$LaFeO_3$ (50 mL of EBT of 70 mg/L, 0.4 g sorbent at 25°C)

Sorbent	First-order		Second-order		Intraparticle diffusion	
	k_1 (1/min)	R^2	k_2 (g/mg/min)	R^2	K_i	R^2
ACSB	3.22×10^{-2}	0.88	1.42×10^{-2}	0.98	2.89×10^{-1}	0.82
ACSB@$LaFeO_3$	1.58×10^{-2}	0.83	4.54×10^{-2}	0.85	3.03×10^{-1}	0.89

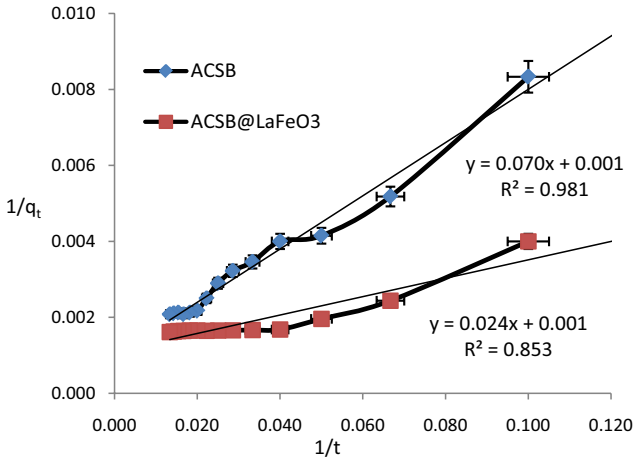

Fig. 9. Pseudo-second-order kinetic model for adsorption of EBT by ACSB and ACSB@$LaFeO_3$ (50 mL of EBT of 70 mg/L, pH 3, and 0.4 g sorbent at 25°C).

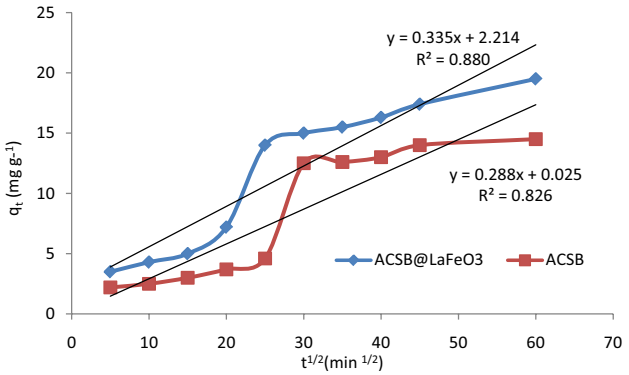

Fig. 10. Intraparticle diffusion model for adsorption of EBT by ACSB and ACSB@$LaFeO_3$ (50 mL of EBT of 70 mg/L, pH 3, and 0.4 g sorbent at 25°C).

The Temkin isotherm is usually used for heterogeneous surface energy systems.

Temkin isotherm contains a factor that clearly shows the interactions between the adsorbent and adsorbate. The Temkin isotherm is written in Eqs. (10) and (11):

$$q_e = \frac{RT}{b}\ln K_t + \frac{RT}{b}\ln C_e \tag{10}$$

$$q_e = B_t \ln K_t + B_t \ln C_e \tag{11}$$

where B_t (J/mol) is Temkin's constant and is related to the temperature of adsorption and B_t (kJ/mol) is heat of sorption. b is Temkin isotherm parameters. K_t is the constant of Temkin isotherm (L/g), R is the universal constant of gases (8.314 J mol^{-1} K^{-1}), and T is absolute temperature (K).

The agreement between the mathematical models and experimental points was evaluated using R^2, χ^2 (non-linear analysis chi-square test).

$$\chi^2 = \sum \frac{\left(q_t - q_{tm}\right)}{q_{tm}} \tag{12}$$

where q_t is the adsorption capacity of the adsorbate at a given time and q_{tm} is the adsorption capacity of the adsorbate at a given time from the corresponding model.

By comparing the values of R^2 and χ^2 the Langmuir model better described the adsorption of EBT (Table 2). This evidences that the adsorption of EBT was monolayer adsorption. Table 3 shows the comparison of adsorption capacities for different carbon materials as sorbents.

3.5. Comparison of EBT removal with different adsorbents

The different adsorption parameters for ACSB@$LaFeO_3$ for the removal of EBT dye have been compared with those of other adsorbents reported in literature and the values of adsorption capacities (q_{max}) have been listed in Table 4. Therefore, it can be noteworthy that the ACSB@$LaFeO_3$ has important potential to removal EBT from aqueous solution. Table 4 shows comparison of adsorption kinetic and isotherm parameters for different carbon materials.

3.6. Adsorption thermodynamics

The thermodynamic parameters such as Gibbs free energy $\Delta G°$, enthalpy $\Delta H°$, and entropy $\Delta S°$ were calculated at different temperatures (15°C–75°C) by using the following equations:

$$\Delta G° = -RT\ln K_d \tag{13}$$

$$\Delta G° = \Delta H° - T\Delta S° \tag{14}$$

$$\ln K_d = \frac{\Delta S°}{R} - \frac{\Delta H°}{RT} \tag{15}$$

$$K_d = \frac{q_e}{C_e} \tag{16}$$

Table 2
Langmuir, Freundlich and Temkin constants for the adsorption of EBT onto by ACSB and ACSB@$LaFeO_3$

Sorbent	Freundlich				Langmuir				Temkin	
	K_F	n	R^2	χ^2	q_m (mg/g)	K_L (L/mg)	R^2	χ^2	R^2	K_t
ACSB	7.1×10^{-2}	–1.5	0.942	5.45	10	6.25×10^{-2}	0.952	1.25	0.904	11.27
ACSB@$LaFeO_3$	1.6×10^{-2}	–3.1	0.882	7.6	16.4	3.1×10^{-1}	0.935	0.98	0.892	10.86

Table 3
Comparison of adsorption parameters for different carbon materials as sorbents

Sorbent	Adsorption capacity (mg/g)	Reference
Carbon almond shell (CAS)	288.57	[14]
Carbon orange peel (COP)	166.7	[14]
Activated carbon derived from date palm petiole	32	[20]
Peanut shell	40	[25]
Activated carbon prepared from *Tridax procumbens*		[26]
Graphene	70	[27]
Acid-modified graphene	102	[27]
Magnetite-impregnated almond shell	33	[42]
Untreated almond shell	29.4	[42]
Activated carbon prepared from waste rice hulls	4.89	[32]
Hazelnut shell	8.28	[43]
Walnut shell	8.01	[43]
ACSB@$LaFeO_3$	910	In this study

Table 4
Comparison of adsorption parameters for EBT by different adsorbents

Sorbent	Reaction order	Isotherm model	Adsorption capacity (mg/g)	pH	Reference
Encalyptus bark	1	L		2, 8	[44]
Mg Al calcined layered double hydroxides	2	L	419	2	[45]
CoAl calcined layered double hydroxides	2	L	540	2	[45]
Ni Fe calcined layered double hydroxides	2	L	132	2	[45]
$NiFe_2O_4$ magnetic nanoparticles	2	L	47	6	[46]
Bentonite carbon Composite	2	F	–	1	[47]
ACSB@$LaFeO_3$	2	L	910	3	In this study

where R is the universal gas constant (8.314 J mol^{-1} K^{-1}), T is the absolute temperature in Kelvin, $K_d = q_e/C_e$ is the distribution coefficient. The values of $\Delta H°$ and $\Delta S°$ were determined from the slope and intercept of the plot of $\ln K_d$ vs. $1/T$ then the value of $\Delta G°$ was calculated using Eq. (11) (Table 5).

The negative $\Delta G°$ value suggests that the adsorption of EBT is a spontaneous and feasible thermodynamically. With increasing of temperature from 15°C to 65°C the negative $\Delta G°$ value increased. This indicates that the adsorption process of EBT onto sorbents is more favorable at higher temperatures. The positive $\Delta H°$ value indicates that the adsorption phenomenon is an endothermic process. The positive value of $\Delta S°$ suggests that the adsorption leads to the decreasing order at the adsorbent–solution interface during the process of adsorption. Generally, a value of $\Delta G°$ in between 0 and −20 kJ/mol is consistent with electrostatic interactions between adsorption sites and the adsorbing ion.

3.7. ACSB@$LaFeO_3$ reuse studies

Desorption study of pollutant is helpful for the recycling of adsorbents. To increase the use of the efficiency of the prepared ACSB@$LaFeO_3$ nanocomposite, desorption, and regeneration of the EBT loaded ACSB@$LaFeO_3$ was investigated. Regeneration requires proper selection of eluent, which strongly depends on the type of adsorbent.

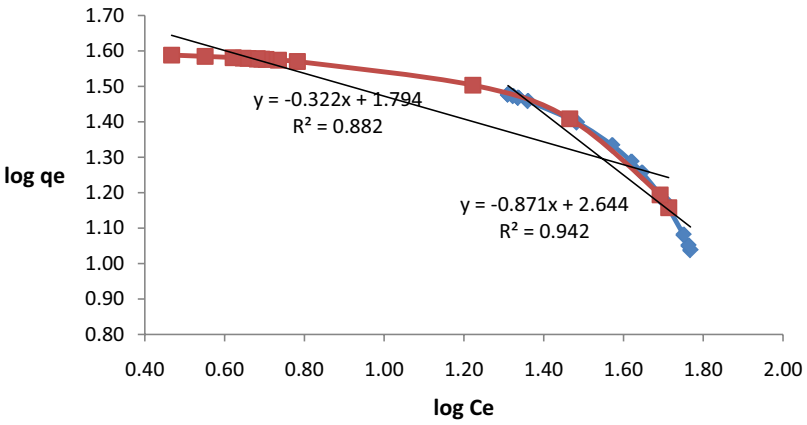

Fig. 11. Frendlich isotherm model for adsorption of EBT by ACSB and ACSB@$LaFeO_3$ (50 mL of EBT of 70 mg/L, 0.4 g sorbent at 25°C).

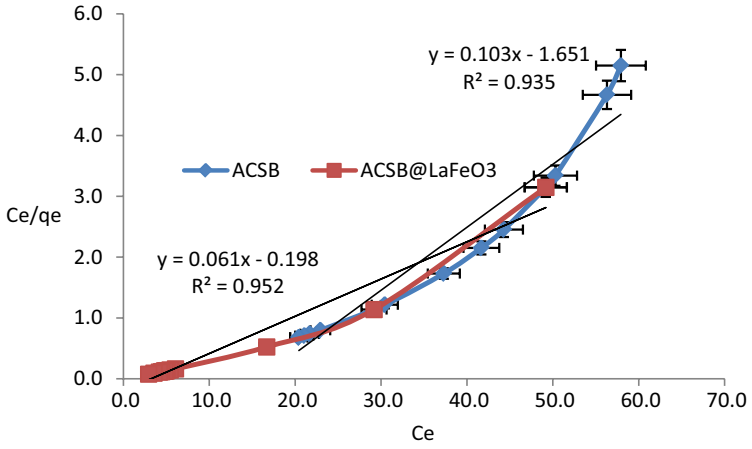

Fig. 12. Langmuir isotherm model for adsorption of EBT by ACSB and ACSB@$LaFeO_3$ (50 mL of EBT of 70 mg/L, 0.4 g sorbent at 25°C).

Table 5
Thermodynamic parameters for adsorption of EBT onto by ACSB and ACSB@$LaFeO_3$

Absorbent	$\Delta S°$	$\Delta H°$	$\Delta G°$	T (K)
	(J/mol/K)	(kJ/mol/K)	(kJ/mol/K)	
ACSB	27.53	5.318	–2.46	288
			–2.61	293
			–2.75	298
			–2.88	303
			–3.01	308
			–3.28	318
			–3.56	328
			–3.836	338
ACSB@$LaFeO_3$	42.52	6.842	–5.25	288
			–5.466	293
			–5.670	298
			–6.02	303
			–6.1	308
			–6.52	318
			–6.94	328
			–7.36	338

The chosen eluent must be operative, harmless to the adsorbent, non-polluting, and economic. On behalf of these purposes, in this study, for reusability of the ACSB@$LaFeO_3$ 0.1 M of NaOH, HCl, CH_3COOH, and deionized water were used. The results showed that HCl 0.1 M had higher desorption efficiency compared with other desorption solutions (Fig. 13). Desorption and regeneration of ACSB@$LaFeO_3$ nanocomposite were not decreased noticeably with three numbers of cycles, suggesting the application of this nanocomposite for the adsorptive removal of EBT.

4. Conclusion

Activated carbon obtained from sugar beet pulp via physical activation using calcination at 800°C was prepared (ACSB). The nanocomposite of ACSB and $LaFeO_3$ was prepared by sol–gel method (ACSB@$LaFeO_3$) and characterized. The surface area of ACSB, LaFeO3, and ACSB@$LaFeO_3$ were determined 825, 15, and 780 m^2/g, respectively. ACSB@$LaFeO_3$ was verified as a sorbent for removal of EBT from aqueous solutions. Adsorption of EBT dependent on the solution pH and the optimum pH value for the better adsorption was found to be 3.0. The adsorption kinetics indicated that pseudo-second-order kinetic model fits well with the experimental data. Adsorption equilibrium data

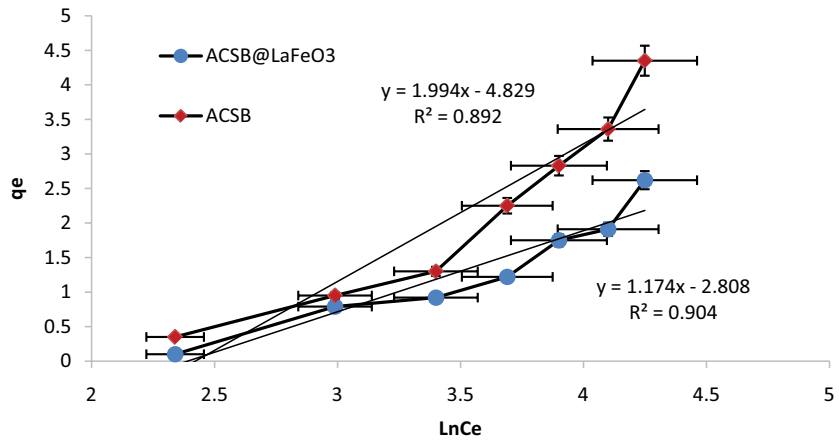

Fig. 13. Temkin isotherm model for adsorption of EBT by ACSB and ACSB@$LaFeO_3$ (50 mL of EBT of 70 mg/L, 0.4 g sorbent at 25°C).

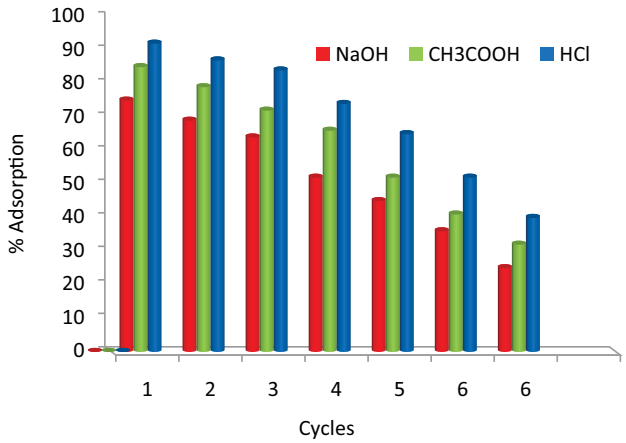

Fig. 14. Regeneration of ACSB@$LaFeO_3$ (50 mL of EBT of 70 mg/L, 0.4 g sorbent at 25°C).

was better described by the Langmuir isotherm model than the Freundlich and Temkin isotherm models. The adsorption capacity of EBT for ACSB and ACSB@$LaFeO_3$ was found to be 550 and 910 mg/g, respectively. The ACSB@$LaFeO_3$ had a simple preparation method using the cheap waste of sugar beet pulp. It acts as an effective and reusable sorbent for dye removal from aqueous solution.

Acknowledgments

The authors are grateful for the financial support provided by Laboratory of Chemistry department of Islamic Azad University of Yazd (IAUY).

References

[1] D. Li, J. Yan, Z. Liu, Z. Liu, Adsorption kinetic studies for removal of methylene blue using activated carbon prepared from sugar beet pulp, Int. J. Environ. Sci. Technol., 13 (2016) 1815–1822.
[2] W. Liu, L. Liu, C. Liu, Y. Hao, H. Yang, B. Yuan, J. Jiang, Methylene blue enhances the anaerobic decolorization and detoxication of azo dye by *Shewanella onediensis* MR-1, Biochem. Eng. J., 110 (2016) 115–124.
[3] V.K. Balakrishnan, S. Shirin, A.M. Aman, S.R. de Solla, J. Mathieu-Denoncourt, V.S. Langlois, Genotoxic and carcinogenic products arising from reductive transformations of the azo dye, Disperse Yellow 7, Chemosphere, 146 (2016) 206–215.
[4] S. Sadri Moghaddam, M.R. Alavi Moghaddam, M. Arami, Coagulation/flocculation process for dye removal using sludge from water treatment plant: optimization through response surface methodology, J. Hazard. Mater., 175 (2010) 651–657.
[5] N. Mokhtar, E.A. Aziz, A. Aris, W.F.W. Ishak, N.S. Mohd Ali, Biosorption of azo-dye using marine macro-alga of *Euchema spinosum*, J. Environ. Chem. Eng., 5 (2017) 5721–5731.
[6] M.F. Abid, M.A. Zablouk, A.M. Abid-Alameer, Experimental study of dye removal from industrial wastewater by membrane technologies of reverse osmosis and nanofiltration, Iran. J. Environ. Health Sci. Eng., 9 (2012) 9–17.
[7] Ö. Ercan, S. Deniz, E.K. Yetimoğlu, A. Aydın, Degradation of reactive dyes using advanced oxidation method, Clean Soil Air Water, 43 (2015) 1031–1036.
[8] F.W. Sindelar, L.F. Silva, V.R. Machado, L.C. dos Santos, S. Stuelp, Treatment of effluent from the agate dyeing industry using photodegradation and electro dialysis processes, Sep. Sci. Technol., 50 (2015) 142–147.
[9] S. Hashemian, A. Dehghanpor, M. Moghahed, $Cu_{0.5}Mn_{0.5}Fe_2O_4$ nanospinels as potential sorbent for adsorption of brilliant green, J. Ind. Eng. Chem., 24 (2015) 308–314.
[10] F. Dehghani, S. Hashemian, A. Shibani, MFe_2O_4 (M = Co, Ni and Zn) ferrite spinel for adsorption of bromophenole red, J. Ind. Eng. Chem., 48 (2017) 36–42.
[11] J. Panda, J.K. Sahoo, P. Kumaranda, S.N. Sahu, M. Samal, S. Kumar Pattanayak, R. Sahu, Adsorptive behavior of zeolitic imidazolate framework-8 towards anionic dye in aqueous media: combined experimental and molecular docking study, J. Mol. Liq., 278 (2019) 536–545.
[12] J. Kumar Sahoo, A. Kumar, J. Rath, T. Mohanty, P. Dash, H. Sahoo, Guar gum-coated iron oxide nanocomposite as an efficient adsorbent for Congo red dye, Desal. Water Treat., 95 (2017) 342–354.
[13] A. Bhatnagar, M. Sillanpaa, Utilization of agro-industrial and municipal waste materials as potential adsorbents for water treatment - a review, Chem. Eng. J., 157 (2010) 277–296.
[14] S. Hashemian, K. Salari, Z. Atashi Yazdi, Preparation of activated carbon from agricultural wastes (almond shell and orange peel) for adsorption of 2-pic from aqueous solution, J. Ind. Eng. Chem., 20 (2014) 1892–1900.
[15] A.R. Satayeva, C.A. Howell, A.V. Korobeinyk, J. Jandosov, V.J. Inglezakis, Z.A. Mansurov, S.V. Mikhalovsky, Investigation of rice husk derived activated carbon for removal of nitrate contamination from water, Sci. Total Environ., 630 (2018) 1237–1245.

[16] Z. Zhang, X. Luo, Y. Liu, P. Zhou, G. Ma, Z. Lei, L. Lei, A low cost and highly efficient adsorbent (activated carbon) prepared from waste potato residue, J. Taiwan Inst. Chem. Eng., 49 (2015) 206–211.
[17] M. Baysal, K. Bilge, B. Yilmaz, M. Papila, Y. Yurum, Preparation of high surface area activated carbon from waste-biomass of sunflower piths: kinetics and equilibrium studies on the dye removal, J. Environ. Chem. Eng., 6 (2018) 1702–1713.
[18] A.F. Hassan, H. Elhadidy, Production of activated carbons from waste carpets and its application in methylene blue adsorption: kinetic and thermodynamic studies, J. Environ. Chem. Eng., 5 (2017) 955–963.
[19] K. Fu, Q. Yue, B. Gao, Y. Wang, Q. Li, Activated carbon from tomato stem by chemical activation with $FeCl_2$, Colloids Surf., A, 529 (2017) 842–849.
[20] N. Khadhri, M. El Khames Saad, M. Ben Mosbah, Y. Moussaoui, Batch and continuous column adsorption of indigo carmine onto activated carbon derived from date palm petiole, J. Environ. Chem. Eng., 7 (2019) 102775, doi: 10.1016/j.jece.2018.11.020.
[21] H. Laksaci, A. Khelifi, B. Belhamdi, M. Trari, Valorization of coffee grounds into activated carbon using physic-chemical activation by KOH/CO_2, J. Environ. Chem. Eng., 5 (2017) 5061–5066.
[22] V.M. Vučurović, R.N. Razmovski, M.N. Tekic, Methylene blue (cationic dye) adsorption onto sugar beet pulp: equilibrium isotherm and kinetic studies, J. Taiwan Inst. Chem. Eng., 43 (2012) 108–111.
[23] Z. Aksu, I.A. Isoglu, Use of dried sugar beet pulp for binary biosorption of Gemazol Turquoise blue-G reactive dye and copper(II) ions: equilibrium modeling, Chem. Eng. J., 127 (2007) 177–188.
[24] E. Hadinejad, S. Hashemian, S.A. Yasini, Comparison of catalytic effect of Fe-MOF and Fe-ZIF for Fenton degradation of Eriochrome black T, Desal. Water Treat., 90 (2017) 180–188.
[25] S. Boumchita, A. Lahrichi, Y. Benjelloun, S. Lairini, V. Nenov, F. Zerrouq, Application of peanut shell as a low-cost adsorbent for the removal of anionic dye from aqueous solutions, J. Mater. Environ. Sci., 8 (2017) 2353–2364.
[26] R.S. Raveendra, P.A. Prashanth, B.R. Malini, B.M. Nagabhushana, Adsorption of eriochrome black-T azo dye from aqueous solution on low cost activated carbon prepared from *Tridax procumbens*, Res. J. Chem. Sci., 5 (2015) 9–13.
[27] A. Khalid, M. Zubair, Ihsanullah, A comparative study on the adsorption of Eriochrome Black T dye from aqueous solution on graphene and acid-modified graphene, Arabian J. Sci. Eng., 43 (2018) 2167–2179.
[28] N. Afifah, R. Saleh, Synthesis, characterization and catalytic properties of perovskite $LaFeO_3$ nanoparticles, J. Phys. Conf. Ser., 710 (2016) 1–8, doi: 10.1088/1742–6596/710/1/012030.
[29] S. Phokha, S. Pinitsoontorn, S. Maensiri, S. Rujirawat, Structure, optical and magnetic properties of $LaFeO_3$ nanoparticles prepared by polymerized complex method, J. Sol-Gel Sci. Technol., 71 (2014) 333–341.
[30] S. Hashemian, M. Monshizadeh, Removal of methylene blue from aqueous solution by nano $LaFeO_3$ particles, Main Group Chem., 12 (2013) 113–124.
[31] Q. Lin, J. Xu, F. Yang, X. Yang, Y. He, The influence of Ca substitution on $LaFeO_3$ nanoparticles in terms of structural and magnetic properties, J. Appl. Biomater. Funct. Mater., 16 (2018) 17–25.
[32] M.D.G. de Luna, E.D. Flores, D.A.D. Genuino, C.M. Futalan, M.W. Wan, Adsorption of Eriochrome Black T (EBT) dye using activated carbon prepared from waste rice hulls - optimization, isotherm and kinetic studies, J. Taiwan Inst. Chem. Eng., 44 (2013) 646–653.
[33] V. Subbaiah Munagapati, D.S. Kim, Adsorption of anionic azo dye Congo red from aqueous solution by cationic modified orange peel powder, J. Mol. Liq., 220 (2016) 540–548.
[34] N. Fiol, I. Villaescusa, Determination of sorbent point zero charge: usefulness in sorption studies, Environ. Chem. Lett., 7 (2009) 79–84.
[35] S. Lagergren, About the theory of so-called adsorption of soluble substances, Kungliga Svenska Vetensk Handl., 24 (1898) 1–39.
[36] Y.S. Ho, G. McKay, Sorption of dye from aqueous solution by peat, Chem. Eng. J., 70 (1998) 115–124.
[37] Y.S. Ho, J.C.Y. Ng, G. McKay, Kinetics of pollutant sorption by biosorbents: review, Sep. Purif. Method, 29 (2000) 189–232.
[38] Y.S. Ho, Review of second-order models for adsorption systems, J. Hazard. Mater., 136 (2006) 681–689.
[39] M. Pan, X. Lin, J. Xie, X. Huang, Kinetic, equilibrium and thermodynamic studies for phosphate adsorption on aluminum hydroxide modified alygorskite nano-composites, RSC Adv., 7 (2017) 4492–4500.
[40] H.M.F. Freundlich, Over the adsorption in solution, J. Phys. Chem., 57 (1906) 385–470.
[41] I. Langmuir, The adsorption of gases on plane surfaces of glass, mica and platinum, J. Am. Chem. Soc., 40 (1918) 1361–1403.
[42] K. Saeed, M. Ishaq, S. Sultan, I. Ahmad, Removal of methyl violet 2-B from aqueous solutions using untreated and magnetite-impregnated almond shell as adsorbents, Desal. Water Treat., 57 (2016) 13484–13493.
[43] H. Hasar, Adsorption of nickel(II) from aqueous solution onto activated carbon prepared from almond husk, J. Hazard. Mater., B97 (2003) 49–57.
[44] P.N. Dave, S. Kaur, E. Khosla, Removal of Eriochrome black-T by adsorption onto encalyptus bark using green technology, Ind. J. Chem. Technol., 18 (2011) 53–60.
[45] M. Zubair, N. Jarrah, M.S. Manzar, M. Al-Harthi, M. Daud, N. Dalhat Mu'azu, S.A.Haladu, Adsorption of eriochrome black T from aqueous phase on MgAl-, CoAl- and NiFe-calcined layered double hydroxides: kinetic, equilibrium and thermodynamic studies, J. Mol. Liq., 230 (2017) 344–352.
[46] F. Moeinpour, A. Alimoradi, M. Kazemi, Efficient removal of Eriochrome black-T from aqueous solution using $NiFe_2O_4$ magnetic nanoparticles, J. Environ. Health Sci. Eng., 12 (2014) 112–117.
[47] F. El-Dars, H.M. Ibrahim, H.A.B. Farag, M. Zakaria Abdelwahhab, M.E.H. Shalabi, Adsorption kinetics of bromophenol blue and Eriochrome Black T using bentonite carbon composite material, Int. J. Sci. Eng. Res., 6 (2015) 679–688.